LETTER

doi:10.1038/nature12597

Potential for spin-based information processing in a thin-film molecular semiconductor

Marc Warner[1]†, Salahud Din[2], Igor S. Tupitsyn[3], Gavin W. Morley[1]†, A. Marshall Stoneham[1]‡, Jules A. Gardener[1]†, Zhenlin Wu[2], Andrew J. Fisher[1], Sandrine Heutz[2], Christopher W. M. Kay[4] & Gabriel Aeppli[1]

Organic semiconductors are studied intensively for applications in electronics and optics[1], and even spin-based information technology, or spintronics[2]. Fundamental quantities in spintronics are the population relaxation time (T_1) and the phase memory time (T_2): T_1 measures the lifetime of a classical bit, in this case embodied by a spin oriented either parallel or antiparallel to an external magnetic field, and T_2 measures the corresponding lifetime of a quantum bit, encoded in the phase of the quantum state. Here we establish that these times are surprisingly long for a common, low-cost and chemically modifiable organic semiconductor, the blue pigment copper phthalocyanine[3], in easily processed thin-film form of the type used for device fabrication. At 5 K, a temperature reachable using inexpensive closed-cycle refrigerators, T_1 and T_2 are respectively 59 ms and 2.6 μs, and at 80 K, which is just above the boiling point of liquid nitrogen, they are respectively 10 μs and 1 μs, demonstrating that the performance of thin-film copper phthalocyanine is superior to that of single-molecule magnets over the same temperature range[4]. T_2 is more than two orders of magnitude greater than the duration of the spin manipulation pulses, which suggests that copper phthalocyanine holds promise for quantum information processing, and the long T_1 indicates possibilities for medium-term storage of classical bits in all-organic devices on plastic substrates.

The drive to develop spintronics, through precise control and read-out of electron spins, has provided impetus for both fundamental discoveries and practical devices. Whereas initial studies mainly considered solid-state inorganic materials, recent work has focused on more exotic species, in particular single-molecule magnets[5–8]. These tend to be large, complex molecules possessing many electron spins and magnetic nuclei that induce decoherence. Thus, the longest decoherence times are measured at ultralow temperatures with the single-molecule magnets isolated from each other by dilution into either diamagnetic isomorphous host crystals or in frozen solution[4,9]. The latter approach has also been used for other molecular materials, such as N@C_{60} (atomic nitrogen inside a 60-atom carbon cage; ref. 10), that have intrinsically long decoherence times at ambient temperatures.

However, when considering compatibility with current thin-film-based plastic electronic and optoelectronic technologies, and reliability of manufacturing and usage, the potential of simpler molecules, such as copper phthalocyanine (CuPc; Fig. 1a), that can be produced on an industrial scale and readily processed in thin films both for solar energy[3] and molecular electronics[11] should be explored. Moreover, spin-bearing organic molecules often have low spin–orbit coupling, possess a large Hilbert space with many non-degenerate transitions, and can be customized by chemical modification. These positive attributes have led to newer research assessing the potential of macrocycle materials for both spintronics and quantum information processing[5,6,8]. Here we demonstrate that the decoherence times of CuPc are comparable or superior to those of the best molecular systems and can be maintained even in a device-like film configuration on a readily available plastic substrate, Kapton. We achieve this through organic-molecular-beam deposition, co-depositing CuPc with the structurally isomorphous but diamagnetic free base phthalocyanine (H_2Pc), allowing the spin-carrying CuPc molecules to be spatially separated while still adopting a well-defined crystal α-phase[12]. Co-deposition reduces spin–spin interactions and therefore decreases the decoherence rates in the ensemble, the measurement of which is always performed as the first test of utility for quantum information processing[4,5,13–17]. To constrain the orientation of the CuPc molecules, and thereby reduce the spectral variation due to the powder averaging of the anisotropic CuPc g factor (g), we deposited the 400-nm-thick CuPc:H_2Pc films onto a layer of perylene-3,4,9,20-tetracarboxylic dianhydride. This forces the CuPc and H_2Pc molecules to lie nearly flat on the Kapton[18], with the normal to the molecular plane almost perpendicular to the surface (Fig. 1b).

Figure 1c shows the echo-detected field sweeps (EDFSs) of CuPc thin films for different copper spin concentrations. The EDFS is a measurement of the Hahn echo as a function of applied magnetic field[19]. The broadening of spectral features at higher CuPc concentrations results from the increased electronic dipolar interaction. The peak at approximately 325 mT is due to radicals in the Kapton film and oxygen-centred radicals in H_2Pc (ref. 20).

Figure 1d is a schematic of the energy levels that give rise to the EDFS spectra for a single molecular orientation, with the normal to the molecular plane parallel to the applied field, as in our measurements. These are simulated in EASYSPIN[21] using the Hamiltonian $H = g\mu_B \boldsymbol{BS} + \sum \boldsymbol{IAS}$ (see Methods for details), the two terms of which respectively represent the Zeeman energy for the electrons within the external field $\boldsymbol{B}$ (μ_B, Bohr magneton) and the sum of the various hyperfine interactions[19]. Copper(II) complexes have been studied extensively[22]: for CuPc the electronic spin is $S = 1/2$ and for both naturally occurring copper isotopes (^{63}Cu and ^{65}Cu) the nuclear spin is $I = 3/2$. The hyperfine coupling of ^{63}Cu is defined by the diagonal matrix $\boldsymbol{A}$ with $A_{xx} = A_{yy} = -83$ MHz and $A_{zz} = -648$ MHz in the molecular frame[19] (these values scale for ^{65}Cu according to the ratio between gyromagnetic ratios). The predominant (>99%) naturally occurring nitrogen isotope (^{14}N) has $I = 1$ and the four nearest-neighbour nitrogens have a hyperfine coupling to the d^9 Cu^{2+} of $A_{xx} = 57$ MHz and $A_{yy} = A_{zz} = 45$ MHz (ref. 23). The red arrows in Fig. 1d indicate the allowed transitions, which, as indicated in the first magnified view, cluster into four groups (owing to the interaction with the spin-3/2 copper nuclei) of nine transitions (owing to the four identical spin-1 nitrogen nuclei). The second magnified view shows the expected intensity variation of the transitions (1:4:10:16:19:16:10:4:1).

The decoherence time, T_2, is the time over which a quantum bit, or qubit, can reliably store quantum information[19], and is obtained by incrementally increasing τ, the time difference between π/2- and π-pulses, in the Hahn echo sequence (Fig. 2b, inset) and measuring the decay of the

[1]London Centre for Nanotechnology and Department of Physics and Astronomy, University College London, London WC1H 0AH, UK. [2]London Centre for Nanotechnology and Department of Materials, Imperial College London, London SW7 2AZ, UK. [3]Pacific Institute of Theoretical Physics, University of British Columbia, Vancouver, British Columbia V6T 1Z1, Canada. [4]Institute of Structural & Molecular Biology and London Centre for Nanotechnology, University College London, London WC1E 6BT, UK. †Present addresses: Department of Physics, Harvard University, Cambridge, Massachusetts 02138, USA (M.W.); Department of Physics, University of Warwick, Gibbet Hill Road, Coventry CV4 7AL, UK (G.W.M.); RMD Inc., 44 Hunt Street, Watertown, Massachusetts 02472, USA (J.A.G.). ‡Deceased.

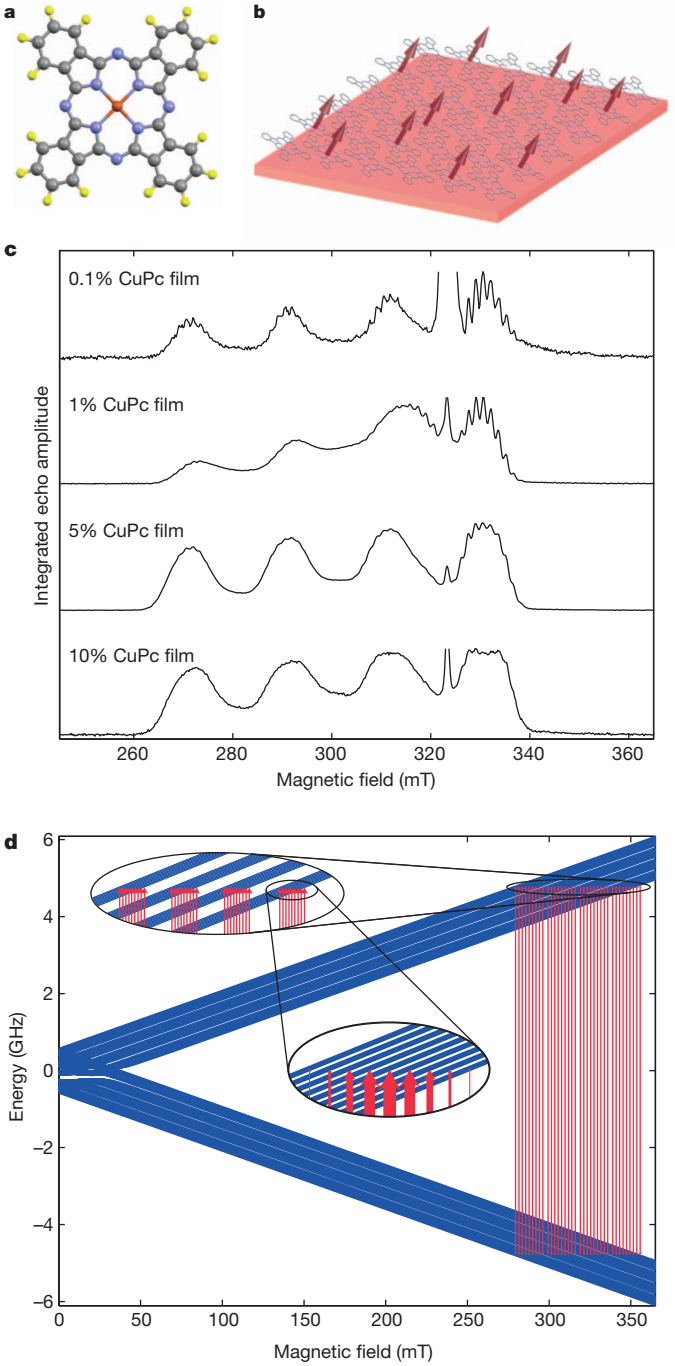

Figure 1 | Copper phthalocyanine films. a, Copper phthalocyanine molecule, containing copper (red), nitrogen (blue), carbon (grey) and hydrogen (yellow) atoms. **b**, Schematic representation of the dilute film, with dispersed electron spins depicted as arrows. For clarity, only a single molecular layer is shown; films used in experiments are 400 nm, or approximately 1,200 layers, thick. **c**, EDFSs collected at 5 K for different copper concentrations. **d**, Energy level structure of the spin Hamiltonian for a single CuPc molecule oriented perpendicular to the magnetic field, with two magnified views showing the copper hyperfine coupling and the nitrogen hyperfine coupling, respectively.

integrated echo[19]. Figure 2a shows the echo decay for varying concentrations of CuPc. The oscillations at early times in the 0.1% CuPc signal are electron spin-echo envelope modulation oscillations caused by coupling to nitrogen nuclear spins[19]. The inset in Fig. 2a shows a comparison of two EDFSs performed at $\tau = 0.4$ and 2.3 μs, respectively, confirming that the echo at long times is from CuPc and not from another spin-carrying defect.

Because the samples are randomly spin-diluted, the local environments of each spin will differ, leading to a distribution of decoherence times, with no single characteristic T_1 or T_2 for a particular concentration. To extract meaningful times we fit the echo decay with $(\alpha + \beta\sin(\omega t + d))\exp(-t/T_2)$ and plot the decay constant as a function of concentration (Fig. 2b). The fit is chosen to allow the extraction of the underlying T_2, the constant that characterizes the exponentially decaying envelope, in the presence of the sinusoidal electron spin-echo envelope modulation oscillations. The dilute limit provides a measure of the intrinsic T_2 of isolated Cu spins for the α-phase samples grown according to this method; different crystal structures can yield different decoherence times because the distances from the copper atoms to electron and nuclear spins that cause relaxation are modified.

Decoherence in electron spin-echo experiments manifests itself through dephasing. For convenience, we introduce a dimensionless decoherence rate, $\gamma = 2\hbar/T_2\Delta_Q$, that is inversely proportional to the number of easily visible coherent oscillations[5]; $\Delta_Q/\hbar = \omega_{EPR} = 9.71$ GHz is the energy gap between the Cu^{2+} $S = 1/2$ qubit states. At very low concentrations, c, of CuPc in H_2Pc, decoherence arises mainly from the local nuclear spins whose motion dephases the dynamics of the electron spins via the hyperfine interaction. At large concentrations, dephasing is dominated by the pairwise dipolar flip-flop processes between the electronic Cu^{2+} spins. For more details, see Methods.

From the fine structure of echo lines in Fig. 1c in the low-c limit, we see that the peaks, corresponding to the four nearest-neighbour nitrogens, strongly overlap. This means that the nuclear spin polarization diffusion is not confined to an individual nitrogen peak and can 'scan' through the entire multiplet of the nitrogen nuclear spin states coupled to the electronic spin of copper (that is, through any one of the four multiplets in the upper left inset in Fig. 1d). For the nuclear spin bath[5], $\gamma_n = 2(E_n/\Delta_Q)^2$, where E_n is the half-width of the above-mentioned multiplet (the limit $E_n \ll \Delta_Q$ is assumed). Knowing the hyperfine couplings and positions of all the nuclear spins in CuPc (ref. 12), we can compute E_n and, correspondingly, the nuclear-induced contribution, $2\hbar/\gamma_n\Delta_Q$, to the total T_2 of the electronic spin. This contribution is represented in Fig. 2b by the green dashed line. The calculated value of E_n ($\sim$1.25 mK $\ll \Delta_Q$) and the value extracted from Fig. 1c at $c = 0.1\%$ agree with each other, and the dominant contribution comes from the four nearest-neighbour nitrogens. Our calculations yield a nuclear-induced dephasing time of 2.2 μs, which is close to the value, $T_2 = 2.6$ μs, that is observed at $c \leq 0.1\%$. At larger concentrations, the dipolar inter-Cu^{2+} processes start to contribute. For $c \leq 10\%$, the electronic spin system is in the dilute limit and the electronic dipolar contribution, E_d, to the echo line half-width is also very small compared with the gap Δ_Q. This allows us to write the electronic decoherence rate, γ_d, in the same form as the nuclear rate, but with E_n replaced by E_d. To calculate E_d, we place CuPc molecules on random sites of a 50-nm-diameter crystalline granule to achieve the desired concentration, and fill the remaining sites with H_2Pc molecules (Methods). Then, after configurational averaging over the CuPc positions, we obtain the electronic pairwise-induced contribution to the total T_2 (Fig. 2b, blue dashed line). The solid red curve shows the total theoretical value, $T_2 = 2\hbar/\Delta_Q(\gamma_n + \gamma_d)$, which we compare with the experimental measurements (blue circles).

To establish experimentally the magnetic field dependence of T_2, we used only diluted CuPc powders, because the smaller resonant cavity of a Q-band spectrometer is not amenable to stacking films. The inset in Fig. 2b demonstrates that in the more dilute α-phase CuPc powders, T_2 is weakly dependent on field, at least up to 1 T.

A lower bound on the population relaxation time, T_1, was measured with an inversion recovery sequence (Fig. 2d, inset) in which t was varied and the integrated echo intensity was monitored[23]. Although this measurement does not strictly include only T_1 effects—there are additional contributions to the echo decay from spectral diffusion—it does reflect the real lifetime of the classical state of the qubit.

Once again, the distribution of environments leads to a signal consisting of a superposition of many exponential decays, with no single

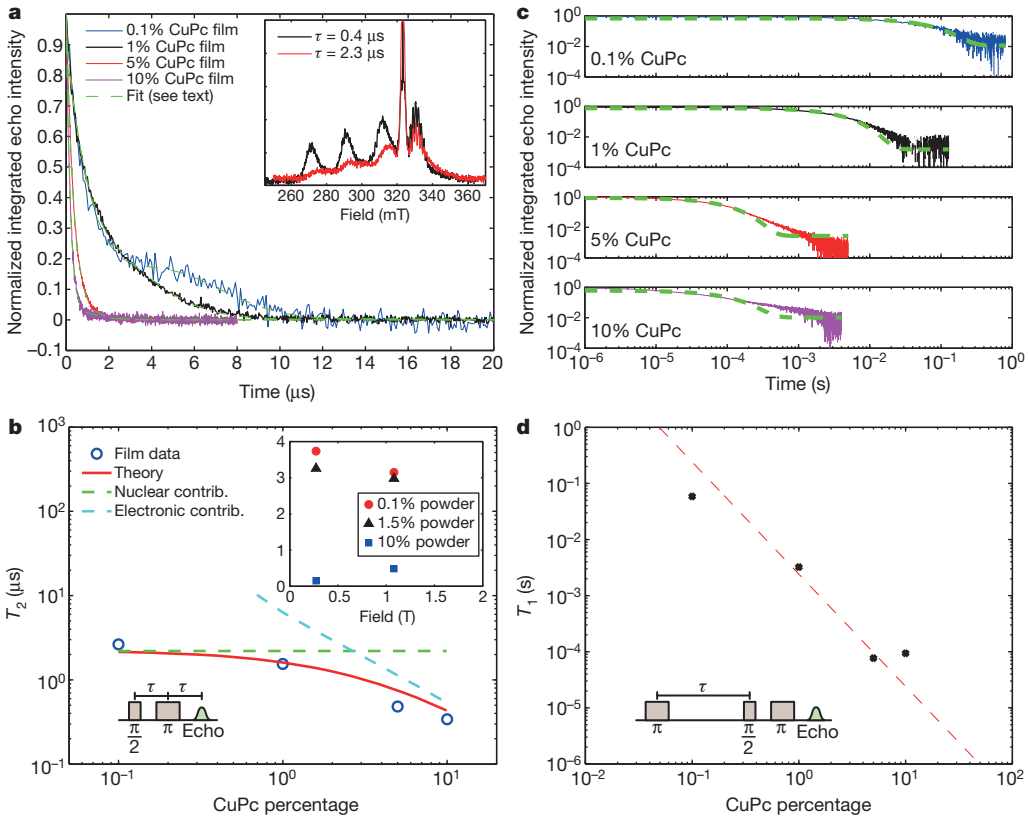

Figure 2 | Concentration dependence of decoherence and relaxation times. **a**, Echo decay with time difference between π/2- and π-pulses for different CuPc concentrations, with fits (see text for details), recorded at 5 K with a 311.5-mT magnetic field. Inset, EDFSs at short and long times showing that the signal is from the CuPc molecules, normalized to the Kapton peak. The differences in shape of the two EDFS spectra indicate a slight field dependence of the relaxation rate. **b**, Experimental T_2 times, extracted from fits, plotted together with theoretical ones as a function of concentration. Lower inset, Hahn echo pulse sequence. Upper inset, respective T_2 values of $(CuPc)_p(H_2Pc)_{1-p}$ powders at 0.273 and 1.08 T, demonstrating the minor field dependence between these values; p is a nominal composition derived from the ratio of starting materials. **c**, Fitted decays (see text for details) of the Hahn echo as part of an inversion recovery sequence recorded at 5 K for different CuPc concentrations. **d**, T_1 values extracted from **c** (symbols), with fit (line; see text for details). Inset, inversion recovery pulse sequence.

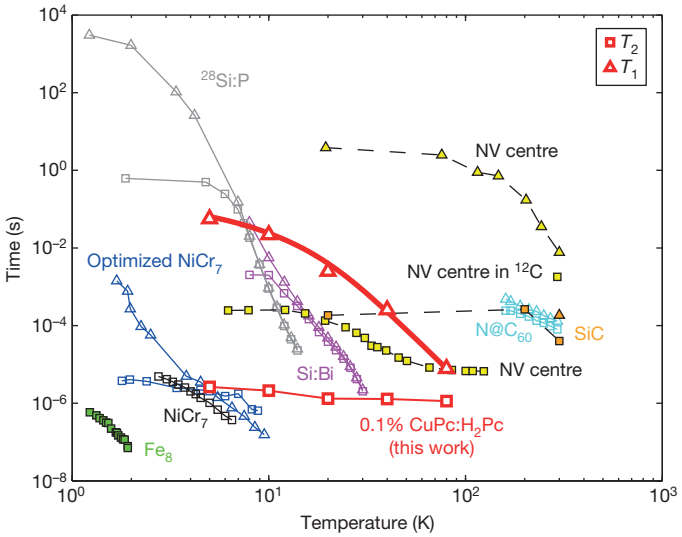

Figure 3 | Temperature dependence of decoherence and relaxation times. T_1 and T_2 versus temperature for 0.1% CuPc:H_2Pc film measured in a 311.5-mT magnetic field, and other common spin qubit systems. It should be noted that the data in this comparison were not all collected at the same magnetic field, but represent the best available comparison from the literature. Data are from ref. 4 ($NiCr_7$), ref. 5 (Fe_8), ref. 9 (optimized $NiCr_7$), ref. 10 ($N@C_{60}$ in CS_2), ref. 13 (^{28}Si:P), ref. 14 (Si:Bi), ref. 15 (nitrogen–vacancy (NV) centre), ref. 16 (nitrogen–vacancy centre in ^{12}C) and ref. 17 (defect in SiC). Lines between points are plotted as guides to the eye, except for that for the T_1 of CuPc:H_2Pc, which was fitted as described in the text.

characteristic decay constant (Fig. 2c). However, by fitting to a single exponential, we can extract a limiting case (for stretched-exponential fits see Extended Data Figs 1, 2 and 3). The fits are imperfect at short times and high concentrations, but improve with dilution, because the probability of the molecules experiencing a similar, isolated, environment increases. The characteristic times derived from the fits at $T = 5$ K are plotted in Fig. 2d, and are approximately proportional to $1/c^2$. Inspection of the decay curves and the corresponding fits shows that these are the shortest times in a distribution of relaxation times; there are also longer times, which become more obvious for higher concentrations. This is expected for the depolarization associated with the non-secular (and, hence, non-magnetization-conserving) part of the dipole–dipole interaction[24], for which the characteristic matrix elements scale as r^{-3} and, hence, as c; the relaxation rate in second-order perturbation theory is therefore proportional to c^2.

To establish whether our films might be useful at or above the boiling point of liquid nitrogen, we measured the temperature dependences of T_1 and T_2. Figure 3 shows these for a 0.1% CuPc film. Experiments, such as ours, that look at the longest decay times naturally select sub-populations of isolated spins. As the temperature is raised, the echo decay becomes closer in character to a mono-exponential decay, indicating—as expected—that differences between spin environments are being averaged away.

In Fig. 3, we also include T_2 (and, where available, T_1) results for a selection of comparable spin qubit candidates in the sense that they use the same control mechanism. Over the easily accessed 5–80 K temperature range, the CuPc:H_2Pc films are superior to all other molecular options, with the exception of $N@C_{60}$ solvated in CS_2 (which makes it

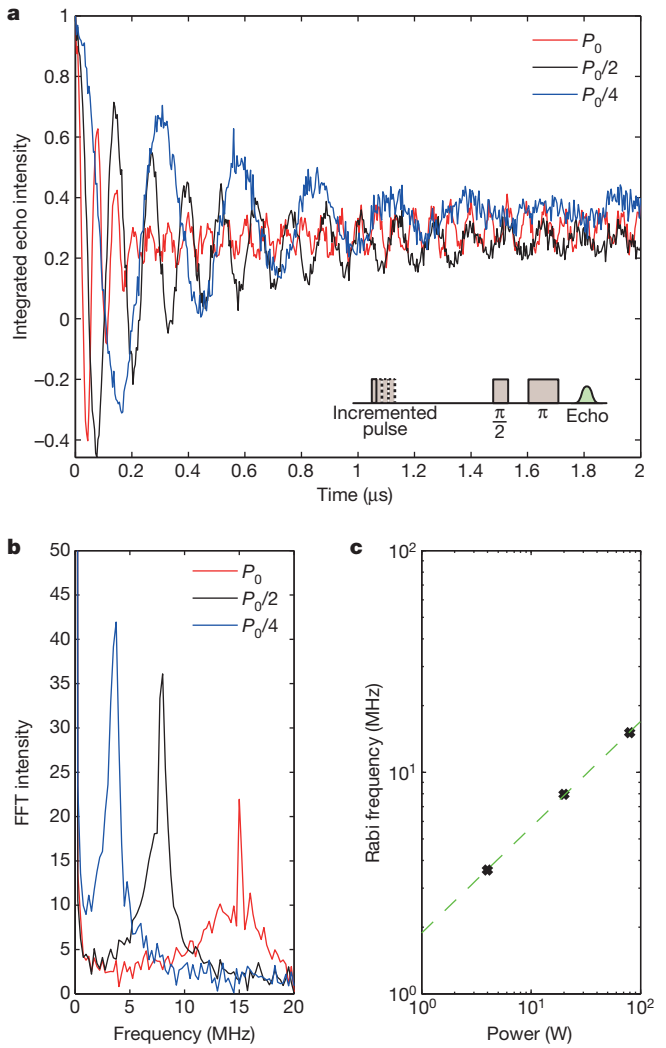

Figure 4 | Controlling a single qubit. **a**, Rabi oscillations of a 0.1% CuPc:H_2Pc film recorded at 5 K and 330.5 mT for different microwave powers. **b**, Fast Fourier transform (FFT) of the Rabi oscillations. **c**, Rabi frequency (symbols) is proportional (line; see text for details) to the microwave field strength, which scales with the square root of the power.

unsuitable for incorporation into devices). Indeed, sufficiently isolated CuPc molecules have decoherence times of approximately 1 μs, even at 80 K, which makes the molecular thin film superior to silicon doped even with the favourable heavy group V element bismuth at temperatures above 30 K (ref. 14). The nitrogen–vacancy centres in diamond have longer relaxation times up to room temperature, but are much more challenging to introduce into the appropriate host in a controlled way. Furthermore, the difference between the T_2 and the long T_1 of the CuPc films demonstrates the potential for optimization, because T_1 provides an upper bound on T_2.

To quantify the T_1 relaxation mechanisms, we fitted the temperature dependence to the form $1/T_1 = a + b/(\exp(-\Delta/T) - 1)$, implying two processes: a temperature-independent spin–spin interaction, where $a = 17.8\ s^{-1}$, and an Orbach process[25]. The energy scale of the Orbach process, Δ, is specified to be 69 K in accordance with literature values for optical phonon excitations in the system[26], and b is then found to be $2.6 \times 10^4\ s^{-1}$. The phonon density of states relevant for decoherence in the weakly bonded stacks of rigid molecules is not expected to be Debye-like; instead, it will be dominated by optical modes associated with motion of the copper atoms relative to their aromatic hosting rings. This fit corroborates the concentration dependence in Fig. 2, because both suggest that T_1 is largely determined by spin–spin interactions at 5 K. The fit could be refined with additional terms[25], but the effects of other processes are not sufficiently distinguished by the data to allow conclusive identification.

Rabi oscillations, that is, the coherent driving of electrons between the two Zeeman-split energy levels, exemplify the ability to manipulate spins both for spintronics and quantum information processing. In Fig. 4a, we show how Rabi oscillations depend on microwave power. The capacity to rotate the qubits arbitrarily to any point on the Bloch sphere is one of the two main requirements for creating universal quantum gates, the other being the ability to entangle qubits. Figure 4c shows that the frequencies of the oscillations, found by Fourier transforming the signal (Fig. 4b), scale linearly with microwave amplitude, which in turn scales with the square root of the power[18]. The decay of the Rabi oscillations is determined by T_2*, which includes both homogeneous and inhomogeneous broadening processes[19], and accordingly includes additional dephasing due to the inhomogeneous magnetic field that each spin encounters. It is therefore shorter than T_2; in this case, $T_2^* = 0.4$ μs at 5 K.

Through further sample optimization, it is likely that the decoherence and relaxation times could be extended. Indeed, our theoretical studies suggest that nitrogen-isotope enrichment is preferable to deuteration here. However, the values of T_1 and T_2 that we measure are already greater than those for single-molecule magnets, which require non-trivial synthesis. For example, T_2 was found to be ~1 μs in optimized Cr_7Ni at 5 K (ref. 9), even with the additional complication of deuteration of both molecule and solvent. In addition, the thin-film samples described here are in a form suitable for device processing[11], can be prepared by a range of deposition techniques[18,27], have the added advantage of being structurally flexible, and are both chemically and thermally robust. The further freedoms to dilute with non-magnetic analogues, to use different chemical motifs to control non-magnetic properties[28], to tune magnetic interactions with minor structural alterations[27,29], to excite at optical frequencies[3] and to inject spins into CuPc with high efficiency[30] make these systems attractive alternatives even to conventional inorganic semiconductors, for which exceptional care must be taken to produce truly random mixtures of magnetic and non-magnetic atoms.

METHODS SUMMARY

To prepare the films, we first grew a 20-nm layer of perylene-3,4,9,20-tetracarboxylic dianhydride on flexible, 25-μm-thick Kapton substrates at 0.2 Å s^{-1} by organic-molecular-beam deposition in a Kurt J. Lesker SPECTROS system with a base pressure of around 5×10^{-7} mbar. On this layer, and without breaking vacuum, 400 nm of CuPc:H_2Pc was grown by co-deposition of CuPc and H_2Pc from two individual Knudsen cells. The concentration, c, of the films is expressed as the percentage of CuPc relative to H_2Pc by mass; the ratio, r, of numbers of molecules—which is useful for calculating distances between spins—is then the product of the concentration and the ratio of H_2Pc mass to CuPc mass, or $0.893c$. All chemicals were purchased from Sigma-Aldrich and purified using two cycles of gradient sublimation.

Films of 0.1% CuPc of area ~9 cm^2, 1% CuPc of area ~7 cm^2, 5% CuPc of area ~6 cm^2 and 10% CuPc of area ~5 cm^2 were sliced and packed into Suprasil EPR tubes. Each tube was aligned with the magnetic field by orienting the sample to maximize the EDFS width, and the X-band (9-GHz) microwave response was measured using a Bruker Elexsys E580 pulsed EPR spectrometer with a Bruker ER 4118X-MD5 dielectric ring resonator. Pulsed Q-band (34-GHz) measurements were performed on the same spectrometer using the 580U-FTQ accessory and an EN 5107D2 Q-band resonator (both from Bruker). The temperature was controlled using an Oxford Instruments CF935 cryostat, allowing studies in the range 4–300 K.

Online Content Any additional Methods, Extended Data display items and Source Data are available in the online version of the paper; references unique to these sections appear only in the online paper.

Received 6 April; accepted 21 August 2013.
Published online 27 October 2013.

1. Sirringhaus, H. *et al.* Two-dimensional charge transport in self-organized, high-mobility conjugated polymers. *Nature* **401,** 685–688 (1999).

2. Dediu, V. A., Hueso, L. E., Bergenti, I. & Taliani, C. Spin routes in organic semiconductors. *Nature Mater.* **8,** 707–716 (2009).
3. Lobbert, G. *Phthalocyanines* in *Ullmann's Encyclopedia of Industrial Chemistry* (Wiley-VCH, 2000).
4. Ardavan, A. *et al.* Will spin-relaxation times in molecular magnets permit quantum information processing? *Phys. Rev. Lett.* **98,** 057201 (2007).
5. Takahashi, S. *et al.* Decoherence in crystals of quantum molecular magnets. *Nature* **476,** 76–79 (2011).
6. Bertaina, S. *et al.* Quantum oscillations in a molecular magnet. *Nature* **453,** 203–206 (2008).
7. Ishikawa, N. Single molecule magnet with single lanthanide ion. *Polyhedron* **26,** 2147–2153 (2007).
8. Hill, S., Edwards, R. S., Aliaga-Alcalde, N. & Christou, G. Quantum coherence in an exchange-coupled dimer of single-molecule magnets. *Science* **302,** 1015–1018 (2003).
9. Wedge, C. J. *et al.* Chemical engineering of molecular qubits. *Phys. Rev. Lett.* **108,** 107204 (2012).
10. Morton, J. J. L. *et al.* Electron spin relaxation of $N@C_{60}$ in CS. *J. Chem. Phys.* **124,** 014508 (2006).
11. Bao, Z., Lovinger, A. J. & Dodabalapur, A. Organic field-effect transistors with high mobility based on copper phthalocyanine. *Appl. Phys. Lett.* **69,** 3066–3068 (1996).
12. Hoshino, A., Takenaka, Y. & Miyaji, H. Redetermination of the crystal structure of alpha-copper phthalocyanine grown on KCl. *Acta Crystallogr. B* **59,** 393–403 (2003).
13. Tyryshkin, A. M. *et al.* Electron spin coherence exceeding seconds in high-purity silicon. *Nature Mater.* **11,** 143–147 (2012).
14. Morley, G. *et al.* The initialization and manipulation of quantum information stored in silicon by bismuth dopants. *Nature Mater.* **9,** 725–729 (2010).
15. Takahashi, S., Hanson, R., van Tol, J., Sherwin, M. S. & Awschalom, D. D. Quenching spin decoherence in diamond through spin bath polarization. *Phys. Rev. Lett.* **101,** 047601 (2008).
16. Balasubramanian, G. *et al.* Ultralong spin coherence time in isotopically engineered diamond. *Nature Mater.* **8,** 383–387 (2009).
17. Koehl, W. F., Buckley, B. B., Heremans, F. J., Calusine, G. & Awschalom, D. D. Room temperature coherent control of defect spin qubits in silicon carbide. *Nature* **479,** 84–87 (2011).
18. Heutz, S., Cloots, R. & Jones, T. Structural templating effects in molecular heterostructures grown by organic molecular-beam deposition. *Appl. Phys. Lett.* **77,** 3938–3940 (2000).
19. Schweiger, A. & Jeschke, G. *Principles of Pulse Electron Paramagnetic Resonance* (Oxford Univ. Press, 2001).
20. Assour, J. & Harrison, S. On origin of unpaired electrons in metal-free phthalocyanine. *J. Phys. Chem.* **68,** 872–876 (1964).
21. Stoll, S. & Schweiger, A. EasySpin, a comprehensive software package for spectral simulation and analysis in EPR. *J. Magn. Reson.* **178,** 42–55 (2006).
22. Stoneham, A. M. The theory of spin relaxation of copper in a Tutton salt crystal. *Proc. Phys. Soc.* **85,** 107 (1965).
23. Finazzo, C., Calle, C., Stoll, S., Van Doorslaer, S. & Schweiger, A. Matrix effects on copper(ii)phthalocyanine complexes: a combined continuous wave and pulse EPR and DFT study. *Phys. Chem. Chem. Phys.* **8,** 1942–1953 (2006).
24. Van Vleck, J. The dipolar broadening of magnetic resonance lines in crystals. *Phys. Rev.* **74,** 1168–1183 (1948).
25. Abragam, A. & Bleaney, B. *Electronic Paramagnetic Resonance of Transition Metal Ions* (Oxford Univ. Press, 1970).
26. Szybowicz, M. *et al.* High temperature study of FT-IR and Raman scattering spectra of vacuum deposited CuPc thin films. *J. Mol. Struct.* **704,** 107–113 (2004).
27. Wang, H. *et al.* Ultralong copper phthalocyanine nanowires with new crystal structure and broad optical absorption. *ACS Nano* **4,** 3921–3926 (2010).
28. Opitz, A., Wagner, J., Brutting, W., Hinderhofer, A. & Schreiber, F. Molecular semiconductor blends: microstructure, charge carrier transport and application in photovoltaic cells. *Phys. Status Solidi A* **206,** 2683–2694 (2009).
29. Heutz, S. *et al.* Molecular thin films: a new type of magnetic switch. *Adv. Mater.* **19,** 3618–3622 (2007).
30. Cinchetti, M. *et al.* Determination of spin injection and transport in a ferromagnet/organic semiconductor heterojunction by two-photon photoemission. *Nature Mater.* **8,** 115–119 (2009).

Acknowledgements S.H. and Z.W. thank EPSRC (EP/F039948/1) for the award of a First Grant. S.H. and S.D. thank Kurt J. Lesker and EPSRC for a CASE award. Work at UCL and Imperial College was supported by the EPSRC Basic Technologies grant Molecular Spintronics (EP/F041349/1 and EP/F04139X/1). G.W.M. is supported by the Royal Society. I.S.T. thanks IARPA, NSERC (grant CNXP 22R81695) and PITP for support.

Author Contributions M.W. conducted the electron spin resonance measurements with input and supervision from G.A. and C.W.M.K. S.D., J.A.G. and Z.W. made and characterized the samples with input and supervision from S.H.. M.W., G.W.M., A.M.S., A.J.F., C.W.M.K. and G.A. analysed data, I.S.T. performed theoretical work, and M.W. wrote the manuscript.

Author Information Reprints and permissions information is available at www.nature.com/reprints. The authors declare no competing financial interests. Readers are welcome to comment on the online version of the paper. Correspondence and requests for materials should be addressed to M.W. (marc.warner@ucl.ac.uk) or G.A. (gabriel.aeppli@ucl.ac.uk).

METHODS

Experimental methods. To prepare the films, a 20-nm layer of perylene-3,4,9,20-tetracarboxylic dianhydride was grown on flexible, 25-μm-thick Kapton substrates at 0.2 Å s^{-1} by organic-molecular-beam deposition in a Kurt J. Lesker SPECTROS system with a base pressure of around 5×10^{-7} mbar. On this, and without breaking vacuum, 400 nm of CuPc:H_2Pc was grown by co-deposition from two individual Knudsen cells. The total rate of deposition onto the substrate was maintained at 1 Å s^{-1}, and the individual rates of CuPc and H_2Pc deposition adjusted depending on the desired stoichiometry of the films. The rates were controlled with quartz crystal monitors placed at the sources and at the substrate. The concentration of the films is expressed as the percentage of CuPc relative to H_2Pc by mass. All chemicals were purchased from Sigma-Aldrich and purified using two cycles of gradient sublimation.

Films of 0.1% CuPc of area ~9 cm^2, 1% CuPc of area ~7 cm^2, 5% CuPc of area ~6 cm^2 and 10% CuPc of area ~5 cm^2 were sliced and packed into Suprasil EPR tubes. Each tube was aligned to the magnetic field by orienting the sample to maximize the EDFS width. Powders were prepared as follows. First, 3 ml of concentrated H_2SO_4 (98%) and 15 ml of IPA were cooled for 10 min in ice water. Then 0.3 g of CuPc or H_2Pc (Sigma-Aldrich; purity, 97%) was dissolved in the acid at a concentration of 18×10^{-6} mol dm^{-3} while stirring continuously. The acid paste was then put drop by drop into the IPA with continuous agitation. The mixture was filtered and washed in distilled water and acetone, and then the precipitate was left to dry on the filter paper for 30 min. The precipitate was finally allowed to dry completely in a desiccator overnight. The yield was estimated to be 50%.

Pulsed X-band (9-GHz) measurements were made with a Bruker Elexsys E580 pulsed EPR spectrometer with a Bruker dielectric ring resonator ER 4118X-MD5. A pulse of 40 ns and a π/2-pulse of 20 ns were used. Pulsed Q-band (34-GHz) measurements were performed on the same spectrometer using the 580U-FTQ accessory and a EN 5107D2 Q-Band resonator (both from Bruker).

In the Rabi pulse sequence, when the attenuation of the microwaves was changed, the detection sequence power was corrected by adjusting the pulse lengths appropriately. The microwave frequency was approximately 9.71 GHz, and the pulse power is specified by the manufacturer to be 0.3 kW at the attenuation used. The temperature was controlled using a CF935 Cryostat, allowing studies in the range 4–300 K.

Theoretical methods. The Cu^{2+} ion in the $C_{32}H_{16}N_8Cu$ molecule has electronic spin $S = 1/2$ and nuclear spin $I^{Cu} = 3/2$. The nitrogens (^{14}N), hydrogens (^{1}H) and carbons (^{12}C) (the naturally occurring isotopes) are characterized by the nuclear spins $I^N = 1$, $I^H = 1/2$ and $I^C = 0$, respectively. The samples used in the experiments are 400-nm thin films of ~50-nm, nearly spherical CuPc:H_2Pc granules. The H_2Pc molecule has the same nuclear spins but lacks the Cu atom at the centre and is thus nonmagnetic. The CuPc:H_2Pc granules have the α-phase brick-stack lattice structure with the lattice constants $a = 12.9$ Å, $b = 3.77$ Å and $c = 12.24$ Å and angles $\alpha = 96.22^\circ$, $\beta = 90.62^\circ$ and $\gamma = 90.32^\circ$ (ref. 12).

The Hamiltonian, describing an ensemble of CuPc molecules in external magnetic field $\boldsymbol{B}$, reads as

$$H = -\mu_B \sum_i \sum_{\mu=x,y,z} g_\mu B^i_\mu S^i_\mu + \sum_{n,i} \sum_{\mu,\nu=x,y,z} A^{ni}_{\mu\nu} I^n_\mu S^i_\nu + \sum_{i<j} \sum_{\mu,\nu=x,y,z} V^{ij}_{\mu\nu} S^i_\mu S^j_\nu \quad (1)$$

where Greek letters indicate space indices, n enumerates nuclear species, and i and j indicate electronic spins. The first and third terms describe the anisotropic electronic Zeeman ($\boldsymbol{B}^i$ is the total field acting on the ith electronic spin) and dipole–dipole interactions between the Cu^{2+} electronic spins in the sample. The second term includes (omitting the electronic spin index) the hyperfine interaction between the electronic and nuclear spins of Cu ($A^{Cu}_{\mu\mu}$); the hyperfine interactions between the electronic spin of copper and the nuclear spins of the four nearest-neighbour nitrogens in one molecule ($A^N_{\mu\mu}$); and the dipole–dipole interactions between the copper electronic spin and all the nuclear spins, both in the local molecule and in the rest of sample ($A^n_{\mu\nu}$). There are other terms in the Hamiltonian, describing internuclear interactions, nuclear quadrupolar terms and so on, but their effects are negligibly small (see below). The components of the anisotropic g factor and the strengths of the hyperfine interactions in CuPc are known[23]: $g_z = 2.1577$, $g_x = g_y = 2.039$; $A^{Cu}_{zz} = -648$ MHz, $A^{Cu}_{xx} = A^{Cu}_{yy} = -83$ MHz; $A^N_{xx} = 57$ MHz, $A^N_{yy} = A^N_{zz} = 45$ MHz. The positions of all atoms within CuPc are also known[12]. The hybridization between the electronic orbitals of the copper ion and ligands decreases the effective value of the copper's electronic spin in CuPc. This effect is described by the covalency parameter, α^2, and in CuPc it varies between 0.72 and 0.77 (ref. 23). In our calculations, we use $\alpha^2 = 0.74$.

Decoherence. Because Cu^{2+} has $S = 1/2$, the spin–phonon channel of decoherence is absent and two relevant decoherence mechanisms here are related to dephasing of the electronic spin dynamics due to interactions with the nuclear and electronic spin baths (precession of local nuclear spins around the changing directions of the local field, created by the electronic spin, and flip-flop transitions in pairs of the dipole-coupled electronic spins). The essential parameter is a dimensionless decoherence rate, γ, which is inversely proportional to the number of coherent oscillations before decoherence sets in and is related to the decoherence time by $T_2 = 2\hbar/\gamma\Delta_Q$, where Δ_Q is the energy gap between the electronic spin states. Details on the corresponding mechanisms with application to quantum nanomagnets can be found in refs 5, 31, 32.

Nuclear spin bath. The half-width, E_n, of the Gaussian multiplet of nuclear spin states coupled to the electronic spin of Cu^{2+} is given by

$$E_n^2 = \sum_k \frac{(\omega_k^{||})^2 I_k(I_k+1)}{3}$$

where $\omega^{||}{}_k$ are the differences between the energies of interaction of the electronic spin and the kth nuclear spin when the electronic spin is in the two different (qubit) states[32,33]. They depend on positions of nuclear spins and hyperfine couplings. With this information, E_n can be calculated for any value of the external magnetic field or, equivalently, for any value of the gap $\Delta_Q = \hbar\omega_{EPR}$. For a CuPc molecule with naturally occurring isotopes at $\Delta_Q = 9.71$ GHz, we obtain $E_n \approx 1.25$ mK, with the dominant contribution from the four nearest-neighbour nitrogens. The calculated E_n and the experimentally measured half-width of the echo line at $c = 0.1\%$ (extracted from Fig. 1c) agree with each other. This correspondence indicates that the calculation captures the essential physics, and thus justifies neglecting other terms (internuclear and so on) in the Hamiltonian (equation (1)). In the limit $E_n \ll \Delta_Q$, the nuclear dimensionless decoherence rate, γ_n, can be obtained perturbatively[32,33], yielding $\gamma_n = 2(E_n/\Delta_Q)^2$. The nuclear-spin-bath-induced contribution to the electronic decoherence time, T_2, at $k_BT \gg E_n$ is temperature independent. It is also independent of the CuPc concentration.

Electronic spin bath. The electronic dipolar contribution, E_d, to the echo line half-width increases with the concentration of CuPc molecules, and to calculate it we use the Van Vleck method[24]. The electronic decoherence times in this work were measured at $5\,K < T < 80\,K$, which is very large compared with all the other parameters. Thus, it is safe to consider the limit of infinite temperatures. In this limit, the generalized expression for the Van Vleck second moment with $\boldsymbol{B}$ parallel to $\hat{\boldsymbol{Z}}$ and for an anisotropic g factor is

$$E_d^2 = \frac{1}{N_m} \sum_{i<j} \frac{W_{ij}^2 S(S+1)}{3}$$

where

$$W_{ij} = \frac{1}{2}(2g_{||}^2 + g_\perp^2)\frac{\mu_0}{4\pi}\frac{\mu_B^2}{|r_{ij}|^3}\left(1 - \frac{3z_{ij}^2}{|r_{ij}|^2}\right)$$

and N_m is the number of CuPc molecules, $|r_{ij}|$ is the distance between two molecules and the dipolar sum can be calculated numerically for any sample geometry. We limit our consideration to one 50-nm granule, varying the number of CuPc molecules with concentration and randomly placing them on the lattice. The remaining sites of the α-phase lattice are occupied by nonmagnetic H_2Pc molecules. The configurational averaging (that is, averaging over the positions of the CuPc molecules) corresponds to sampling a large ensemble of granules. Owing to the templating effect, molecules in all the granules are nearly parallel to the Kapton film, which makes the orientational averaging unnecessary. In small α-phase CuPc:H_2Pc granules, the second momentum always remains finite, decreasing together with concentration (no long-tail divergences). At concentrations $c \leq 10\%$, the electronic spin system is in the dilute limit, characterized by $E_d \ll \Delta_Q$. In this limit, we can follow the case of the nuclear-spin-bath approach and obtain the electronic dimensionless decoherence rate perturbatively in the form $\gamma_d = 2(E_d/\Delta_Q)^2$. At $k_BT \lesssim \Delta_Q$, the electronic dipolar-flip-flop-induced contribution to the total electronic T_2 is temperature dependent.

31. Morello, A., Stamp, P. C. E. & Tupitsyn, I. S. Pairwise decoherence in coupled spin qubit networks. *Phys. Rev. Lett.* **97,** 207206 (2006).
32. Stamp, P. C. E. & Tupitsyn, I. S. Crossover in spin-boson and central spin models. *Chem. Phys.* **296,** 281–293 (2004).
33. Stamp, P. C. E. & Tupitsyn, I. S. Coherence window in the dynamics of quantum nanomagnets. *Phys. Rev. B* **69,** 014401 (2004).
34. Barbon, A., Brustolon, M., Lisa Maniero, A., Romanelli, M. & Brunel, L.-C. Dynamics and spin relaxation of tempone in a host crystal. An ENDOR, high field EPR and electron spin echo study. *Phys. Chem. Chem. Phys.* **1,** 4015–4023 (1999).
35. Romanelli, M. & Kevan, L. Evaluation and interpretation of electron spin-echo decay part I: rigid samples. *Concepts Magn. Reson.* **9,** 403–430 (1997).

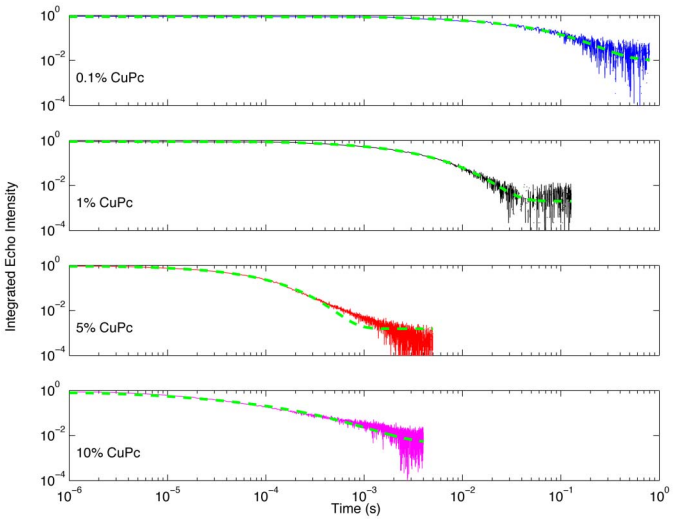

Extended Data Figure 1 | Stretched-exponential T_1 fits. Inversion recovery echoes for varying CuPc concentrations fitted with stretched exponentials. The T_1 decay of each echo magnitude can also be fitted to a stretched exponential, $A\exp(-x/k)^{\beta}$, which is a form characteristic of the random environment that the CuPc molecules experience. In particular, the more isolated molecules will show slower relaxation[34]. However, because the stretched exponential is a phenomenological fit, it must be interpreted with care, particularly in cases where the underlying distribution of relaxation times is highly non-trivial. This is the case in this work, where relaxation times depend strongly on long-range dipolar interactions and, therefore, the finite size of the crystallites[35].

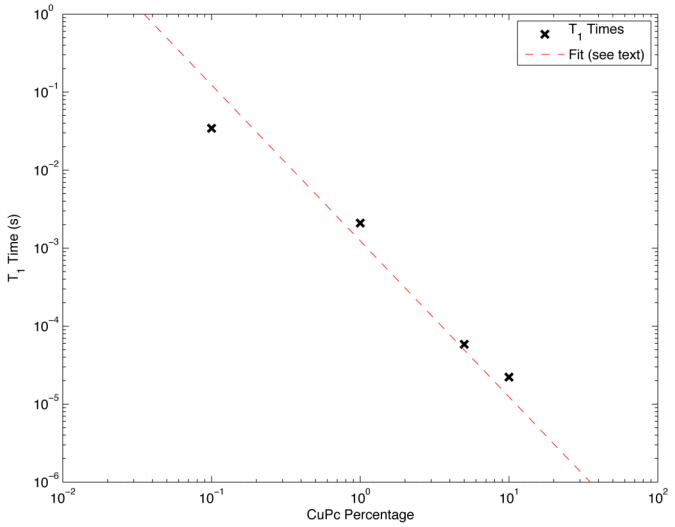

Extended Data Figure 2 | Decay times of stretched-exponential fits. Decay times extracted from the fits in Extended Data Fig. 1 and plotted against CuPc concentration. The concentration dependence of T_1 is not greatly affected by the change in fit. This allows the interpretation of the data based on the simpler mono-exponential fits (main text).

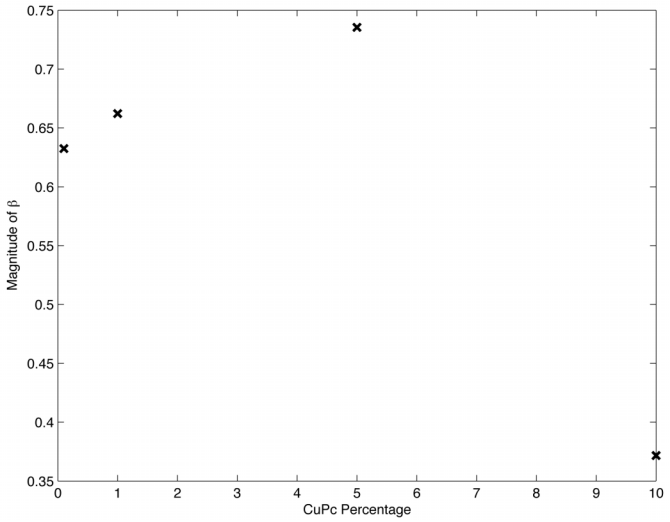

Extended Data Figure 3 | Power-law exponents of stretched-exponential fits. Magnitudes of the power-law exponent, β, in the fits in Extended Data Fig. 2 plotted against CuPc concentration. In a uniform environment, $\beta = 1$ for the population of spins. The greater is the deviation from this value, the larger is the proportion of long-lived isolated spins relative to the average.